Refraction of nonlinear light beams in nematic liquid crystals

Refraction of Nonlinear Light Beams in Nematic Liquid Crystals

Gaetano Assanto,[1] Noel F. Smyth,[2] and Wenjun Xia[2]
[1] *NooEL— Nonlinear Optics and OptoElectronics Lab*
Via della Vasca Navale 84, 00146 Rome, Italy
email: assanto@uniroma3.it
[2] *School of Mathematics and Maxwell Institute for Mathematical Sciences*
The King's Buildings, University of Edinburgh
Edinburgh, Scotland, EH9 3JZ, U.K.
emails: N.Smyth@ed.ac.uk and W.J.Xia@sms.ed.ac.uk
(Dated:)

We use modulation theory to analyze the interaction of optical solitons and vortices with a dielectric interface between two regions of nematic liquid crystals. In the analysis we consider the role of nonlocality, anisotropy and nonlinear reorientation and compare modulation theory results with numerical results. Upon interacting with the interface, nematicons undergo transverse distortion but remain stable and eventually return to a steady state, whereas vortices experience an enhanced instability and can break up into bright beams or solitary waves.

I. INTRODUCTION

Nematicons [1–3], self-confined light beams in nematic liquid crystals, have become an excellent playground for designing and demonstrating all-optical switching and routing circuits in reconfigurable settings and guided-wave formats. Following their demonstration in planar voltage-assisted cells [4], the spatial routing of nematicons and the associated waveguides [5, 6] have been successfully pursued by exploiting birefringent walkoff [7–12], soliton-soliton interactions [13–16], lensing effects [17–19], boundary effects [20–23] and refraction and total internal reflection [24–28]. The latter approach, relying on an interface between two dielectric regions of nematic liquid crystals, provided the most striking results in terms of angular steering, with spatial solitons and associated waveguides being steered by angles as large as 40 degrees in geometries with voltage biases across the thickness, and up to 55 degrees for in-plane steering with interdigitated electrodes [29, 30]. Due to the intrinsic anisotropy of nematic liquid crystals, however, two regions separated by an interface and defined by distinct applied voltages exhibit different properties in terms of both refractive indices for the extraordinary field polarization and birefringent walkoff. In addition, the nonlocal medium response and the graded character of the transition layer between two regions bring about a significant interaction of the beam with both media even upon total internal reflection, leading to an appreciable field penetration beyond the interface and, consequently, large lateral shifts [25]. The typical geometry experimentally adopted for the observation of refraction and total internal reflection of self-confined optical beams in reorientational nematic liquid crystals is sketched in Fig. 1, with reference to a planar cell with the molecular director prealigned along p and a nematic layer (E7) of thickness $100\mu m$. By acting on the sign of the bias mismatch between the two dielectric regions, the extraordinary polarized incident beam giving rise to the nematicon could impinge on the interface from an optically rarer or denser region, eventually undergoing total internal reflection at incidence angles above the critical value [24]. A synopsis of experimental results obtained with a near-infrared input beam at $1.064\mu m$ generating a nematicon in a cell as in Fig. 1 is provided in Fig. 2 for both cases of refraction from region 1 to region 2, Figs. 2 (b)–(d), and total internal reflection from region 1 to region 1, Figs. 2(e)–(f). As the applied voltages are varied independently (around an average value allowing for maximum reorientation [31]) in the two regions, the input medium 1 can be made rarer, $\Delta V < 0V$, or denser, $\Delta V > 0V$, than medium 2, resulting in refraction or reflection, respectively. For a voltage mismatch of about $-0.8V$ refraction caused an angular deviation of the soliton of about 18 degrees, Fig. 2(d), whereas for $\Delta V = +0.8V$ the reflected nematicon changed direction by about 22 degrees, Fig. 2(f). The overall waveguide steering of about 40 degrees is an outstanding result in guided-wave optics, with a negligible amount of power lost from the self-confined beam during the interaction with the interface.

Figure 3 displays a photograph of a nematicon which, undergoing total internal reflection from a denser to a rarer medium, is subject to a large Goos-Hänchen type shift [32] along p [25]. The observed lateral shift can be of the order of mm thanks to the large nonlocality and the graded character of the interface. Figure 3 also shows equivalent numerical and modulation solutions displaying Goos-Hänchen reflection. On noting that the theoretical solutions are displayed in the nondimensional physical (z, y) coordinates of Figure 1, with ξ the y position of the nematicon peak, the theoretical results can be seen to qualitatively match the experimental ones. Converting the theoretical solution shown in Figure 3 to dimensional units [33] gives a Goos-Hänchen shift of around $250\mu m$, compared with the experimental result of around $500\mu m$. The experimental Goos-Hänchen shift is more complicated than the simple theoretical modelling. The beam stays close to the interface for an extended distance. As the interface is graded with a width of $50\mu m$ [25, 27], not the sharp step of the theoretical modelling, close agreement between the experimental

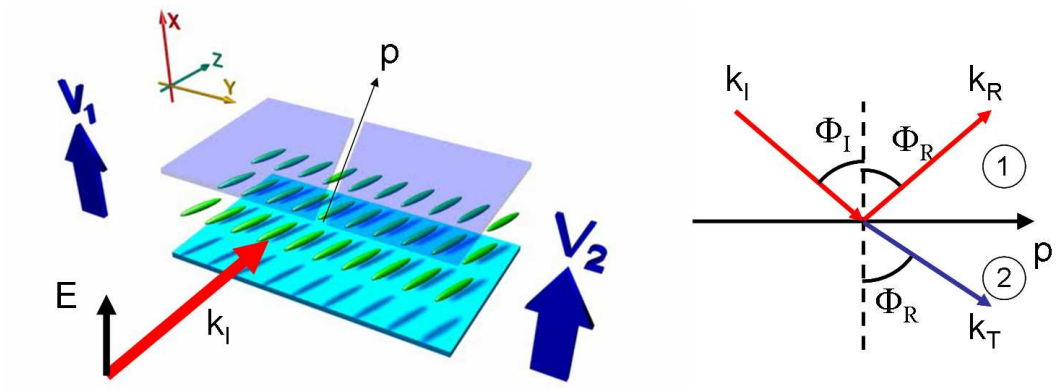

FIG. 1: (Color online) Left: Planar cell with two transparent electrodes at the top and a common ground electrode. Distinct voltage biases V_1 and V_2 can differently tilt the optic axis (molecular director) in the plane xz, therefore defining two dielectric regions 1 and 2 separated by a gap along p. The input beam is extraordinary polarized and impinges on p at an angle, undergoing either refraction (from region 1 to region 2), or total internal reflection (from 1 to 1) depending on the bias mismatch. Right: geometry of the wavevectors across the interface.

and theoretical shifts is not expected, with only order of magnitude agreement expected. Furthermore, the actual shift depends on the power of the beam and the voltage difference across the interface.

The equations governing nonlinear optical beam propagation in nematic liquid crystals form a coupled system of a nonlinear Schrödinger (NLS)-type equation for the optical beam and an elliptic Poisson equation for the medium response. These equations have no exact solitary wave, or other, solutions. While numerical solutions of the governing equations can be found, it has been found that approximate, or modulation, theories give insight into the mechanisms behind nonlinear optical beam evolution, while at the same time giving approximate solutions in good to excellent agreement with full numerical solutions and experimental results. Modulation theory has been found to give solutions in excellent agreement with numerical results for single nematicon evolution [34–37], interacting nematicons [38–41] and the interaction of nematicons with localised refractive index changes [42–45]. It has also been found to give results in excellent agreement with experimental data for nematicon tunnelling through a waveguide [33]. This approximate analytical work on nematicon, or optical solitary waves in a nematic liquid crystal, has been extended to optical vortex evolution and stability in a nematic liquid crystal [46–48], again with excellent agreement with numerical solutions. In this paper we use modulation theory to model refraction and total internal reflection of self-trapped optical beams in nematic liquid crystals in the case of a planar cell with two separate regions defined by independently applied bias voltages. By including walkoff and nonlocality in addition to the reorientational nonlinear response, we are able to reproduce the basic experimental results, as well as the results of full numerical simulations of the pertinent equations. Moreover, we adapt modulation theory to model the case of optical vortices of +1 topological charge propagating in nematic liquid crystals, demonstrating how their instability can be triggered by the interaction with the interface despite the stabilizing role of the nonlocal response. While the latter phenomenon still awaits an experimental demonstration, the previously obtained agreement of modulation theory models with the behaviour of actual nematicons [33] leads us to expect the forthcoming observation of the predicted effects with vortices as well.

II. MODULATION EQUATIONS

Let us consider the propagation of a nonlinear beam of polarised coherent light in a planar nematic liquid crystal cell. The z direction will be taken to be the beam propagation direction down the cell with x the polarisation direction. To overcome the Freédericksz threshold an external, static biasing electric field is applied across the cell to pre-tilt the nematic molecules at an angle ψ_b to the z direction. This external electric field will take two distinct constant values in the (y, z) plane, ψ_{bl} and ψ_{br}, which are separated by the line $y = \mu_1 z + \mu_2$, as in the first experimental reports [24, 25]. In the experiments, the biasing electric field did not have a sharp step discontinuity, but a smooth transition between the two constant values over a distance of the order of the gap between the electrodes generating the fields, this being about $50\mu m$ [25, 27]. As this is small compared with the typical cell width and length, a step discontinuity is an acceptable approximation. In the paraxial approximation the nondimensional system of equations

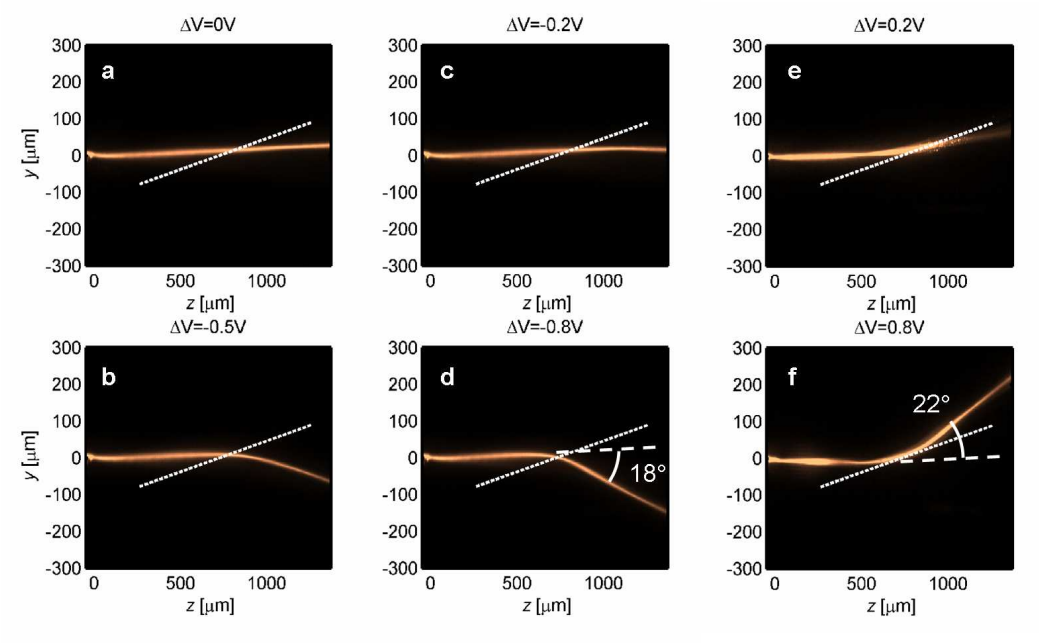

FIG. 2: (Color online) Photographs of a near infrared (1064nm) nematicon excited at $4.5mW$ and interacting with the interface along p, indicated by a dashed line, for various bias mismatches. (a) Nematicon going straight as p separates two optically identical regions; (b) Refraction from a rarer to a denser medium for $\Delta V = -0.5V$; (c), as in (b), but for a smaller index difference, i.e. $\Delta V = -0.2V$; (d), as in (b), but for a larger index difference, i.e. $\Delta V = -0.8V$; (e) total internal reflection from a denser to a rarer region for $\Delta V = +0.2V$; (f), as in (e), but for a larger mismatch $\Delta V = +0.8V$.

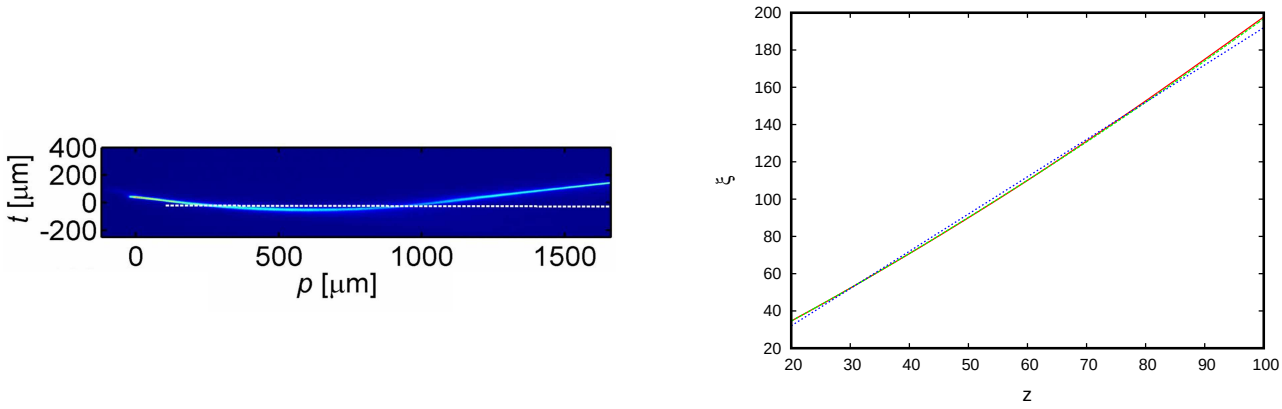

FIG. 3: (Color online) Left: Photograph of a nematicon excited at $1.6mW$ and undergoing total internal reflection from/to an optically denser medium (region 1). The soliton center of mass or beam axis clearly appears to penetrate beyond the nominal interface (dashed line), exhibiting a substantial lateral shift of the order of or larger than mm. Right: Goos-Hänchen reflection from modulation theory. Numerical solution: solid (red) line; modulation solution: dashed (green) line; interface: dotted (blue) line. z (nondimensional): distance down cell, ξ (nondimensional): position of nematicon maximum.

governing the evolution of a nonlinear beam in nematic liquid crystals is [7, 49–51]

$$i\frac{\partial E}{\partial z} - i\Delta\frac{\partial E}{\partial y} + \frac{1}{2}\nabla^2 E + \sin(2\psi_b)\theta E = 0, \tag{1}$$

$$\nu\nabla^2\theta - 2q\theta = -\sin(2\psi_b)|E|^2. \tag{2}$$

Here E is the complex valued envelope of the electric field of the optical beam. The parameter ν measures the elastic response of the nematic and is large, $O(100)$, in the usual experimental regime [33], so that the response of the nematic

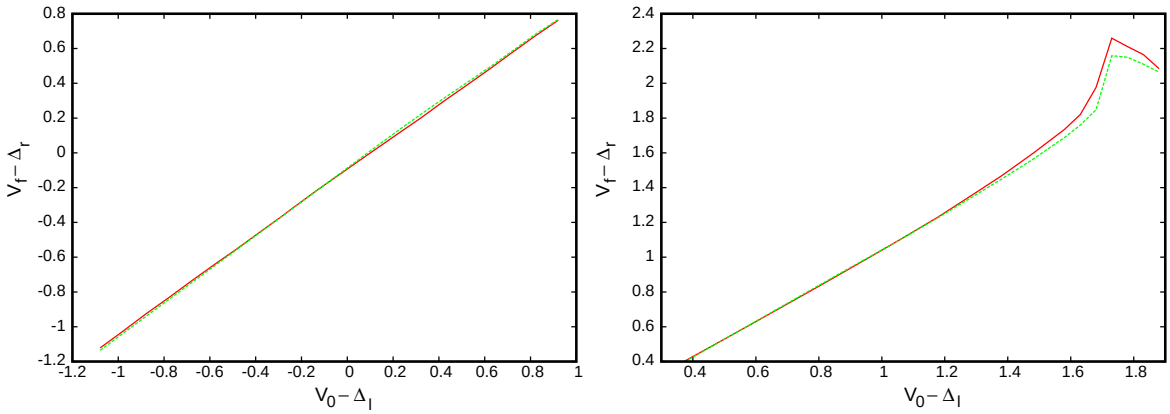

FIG. 4: (Color online) Comparison of propagation constant after refraction $V_f - \Delta_r$ versus incident propagation constant $V_0 - \Delta_l$ for a nematicon as given by the full numerical and modulation solutions. Numerical solution: — (full, red line); modulation solution: – – – (dashed, green line). (a) $a = 4.5$ and $w = 2.5$, with $\nu = 200$, $\psi_{bl} = 0.4$, $\psi_{br} = 0.9$, $q_l = 1.0$, $q_r = 1.3$, $\mu_1 = 2$ and $\mu_2 = -20$, (b) $a = 5$ and $w = 2$, with $\nu = 200$, $\psi_{bl} = 0.8$, $\psi_{br} = 0.6$, $q_l = 1.3$, $q_r = 1.0$, $\mu_1 = 2.0$ and $\mu_2 = -8.0$.

is termed nonlocal as it normally extends far beyond the waist of the beam. The parameter q is proportional to the square of the modulus of the external biasing electric field [49, 50]. The total angle made by the director to the z direction is the pre-tilt plus the extra nonlinear rotation caused by the beam, $\psi = \psi_b + \theta$. For the usual milliwatt beam power levels [4], this extra rotation is rather small, $|\theta| \ll |\psi_b|$. As shown in [52], the governing equations (1) and (2) are valid in this small extra deviation limit. Finally, δ is the walk-off angle between the Poynting vector and the wavevector of the extraordinary beam. In the limit $|\theta| \ll |\psi_b|$ [52]

$$\Delta = \tan\delta = \frac{\Delta n^2 \sin 2\psi_b}{\Delta n^2 + 2n_\perp^2 + \Delta n^2 \cos 2\psi_b}, \tag{3}$$

where $\Delta n^2 = n_\parallel^2 - n_\perp^2$ is the optical birefringence and $n_\parallel$ and $n_\perp$ are the refractive indices for fields parallel and perpendicular to the optic axis, respectively [7]. In the present work the typical values $n_\parallel = 1.6954$ and $n_\perp = 1.5038$ will be used, which refer to the nematic E7 at room temperature in the near infrared at wavelength 1.064 μm [7, 53].

As already mentioned, the refraction of both nematicons and optical vortices will be studied. This refraction is caused by the pre-tilt angle ψ_b taking two distinct values across the line $y = \mu_1 z + \mu_2$, so that the nonlinear refractive index takes two distinct values across this line. We therefore have

$$\psi_b = \begin{cases} \psi_{bl}, & \mu_1 z + \mu_2 < y, \\ \psi_{br}, & y < \mu_1 z + \mu_2 \end{cases}. \tag{4}$$

As the parameter q is related to the square of the pre-tilting field, it also has a jump discontinuity across the line $y = \mu_1 z + \mu_2$

$$q = \begin{cases} q_l, & \mu_1 z + \mu_2 < y, \\ q_r, & y < \mu_1 z + \mu_2 \end{cases}. \tag{5}$$

The nematicon equations (1) and (2) have no exact solitary wave or vortex solutions in either $(1+1)$ or $(2+1)$ dimensions. There are then no exact profiles on which to base a standard "slowly varying" beam analysis. In these circumstances it has been found that the use of appropriate trial functions in an averaged Lagrangian formulation of the governing equations [36, 54, 55] gives results in good agreement with both numerical and experimental data [33, 36, 54]. This approach will be used in the present study of the refraction of nematicons and vortices. In this regard, the nematicon equations (1) and (2) have the Lagrangian formulation

$$L = i\left(E^* E_z - E E_z^*\right) - i\Delta\left(E^* E_y - E E_y^*\right) - |\nabla E|^2 + 2\sin(2\psi_b)\theta|E|^2 - \nu|\nabla\theta|^2 - 2q\theta^2. \tag{6}$$

Suitable trial functions for the electric field and director distribution [36] are

$$\begin{aligned} E &= a\,\mathrm{sech}\,\frac{\sqrt{x^2 + (y-\xi)^2}}{w}\, e^{i\sigma + iV(y-\xi)} + ige^{i\sigma + iV(y-\xi)}, \\ \theta &= \alpha\,\mathrm{sech}^2\,\frac{\sqrt{x^2 + (y-\xi)^2}}{\beta}. \end{aligned} \tag{7}$$

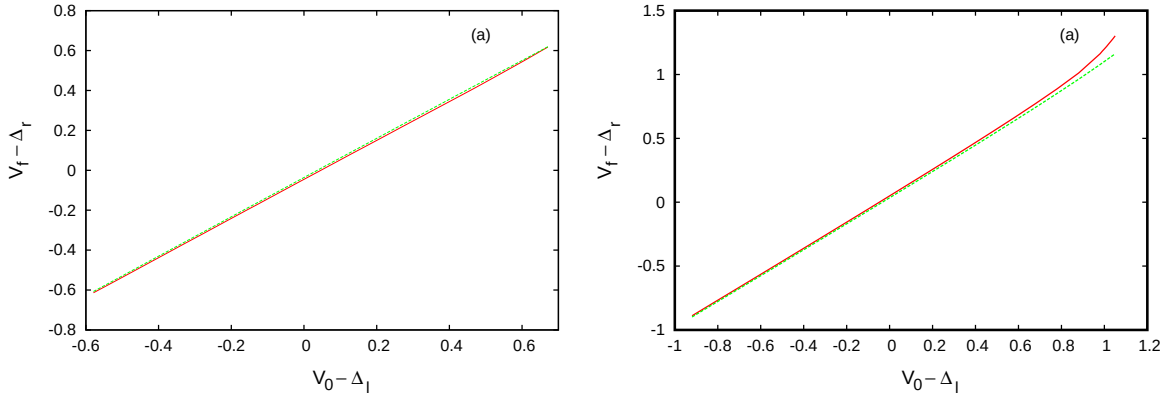

FIG. 5: (Color online) Comparison of the propagation constant after refraction $V_f - \Delta_r$ versus the incident propagation constant $V_0 - \Delta_l$ for a vortex as given by the full numerical and modulation solutions for the initial values $a = 0.15$ and $w = 8.0$, with $\nu = 200$. Full numerical solution: — (red, solid line); modulation solution: – – – (green, dashed line). (a) $\psi_{bl} = 0.4$, $\psi_{br} = 0.9$, $q_l = 1.0$, $q_r = 1.3$, $\mu_1 = 2$ and $\mu_2 = -80$, (b) $\psi_{bl} = 0.8$, $\psi_{br} = 0.4$, $q_l = 1.3$, $q_r = 1.0$, $\mu_1 = 1.5$ and $\mu_2 = -20$.

In these trial functions the amplitude a, waist w, position ξ, propagation constant V, phase σ and g are functions of z, as are the amplitude α and width β of the director distribution. As we have ν large and are in the nonlocal limit, $\beta \gg w$. The first term in the trial function for the electric field consists of a varying solitary wave with the profile of the exact soliton solution of the $(1+1)$ dimensional NLS equation. The second term represents the low wavenumber diffractive radiation which accumulates under the nematicon as it evolves [54]. The existence of this shelf of radiation under the beam can be shown from perturbed inverse scattering theory in the case of the $(1+1)$-D NLS equation [54] or from a perturbation analysis of the governing equations [56, 57]. It is simplest to note that the group velocity of waves for the linearised electric field equation (1) is $\mathbf{c}_g = \mathbf{k}$, where $\mathbf{k}$ is the wavenumber. Hence, low wavenumber waves cannot leave the vicinity of the evolving nematicon. This shelf of radiation then matches to radiation being shed from the nematicon so that it can evolve to a steady state [34, 36, 54]. In the nonlocal limit, this diffractive radiation is shed at a slow rate and is only significant on long z scales [36]. As the refraction of the nematicon occurs on short z scales of $O(100)$, this shed radiation need not be considered here.

In principle, the refraction of an optical vortex can be analysed as for the nematicon. However, the director response to the vortex is more complicated than that for the nematicon due to the nonlocal response causing the optic axis distortion to be non-zero in the vortex core [46–48]. This non-zero perturbed director core, in fact, is the mechanism able to stabilise the vortex [46]. In a similar manner as for the trial function (7) for a nematicon, a suitable trial function for the electric field of the optical vortex is [46]

$$E = are^{-r/w}e^{i\sigma+iV(y-\xi)+i\phi} + ige^{i\sigma+iV(y-\xi)+i\phi}. \tag{8}$$

Here $r^2 = x^2 + (y-\xi)^2$ and ϕ is the polar angle relative to the centre of the vortex $(0, \xi)$. The first term in this trial function is an optical vortex of amplitude $A = awe^{-1}$ and width w, with the second term being the shelf of low wavenumber diffractive radiation under the vortex, which exists for the same reasons as for the nematicon. The simplest manner in which to obtain a suitable trial function for the director distribution is to solve the elliptic director equation (2) in terms of the Green's function G as

$$\theta = -\sin(2\psi_b)\int_{-\infty}^{\infty}\int_{-\infty}^{\infty} G(x,y,x',y')|E(x',y')|^2\,dx'dy'. \tag{9}$$

The Lagrangian for the nematic equations (1) and (2) is then

$$L = i\left(E^*E_z - EE_z^*\right) - i\Delta\left(E^*E_y - EE_y^*\right) - |\nabla E|^2 - \sin^2(2\psi_b)|E|^2\int_{-\infty}^{\infty}\int_{-\infty}^{\infty} G(x,y,x',y')|E(x',y')|^2\,dx'dy'. \tag{10}$$

The trial functions (7) for the nematicon and (8) for the vortex are now substituted into the appropriate Lagrangian, (6) for the nematicon and (10) for the vortex, which are then integrated in x and y from $-\infty$ to ∞ to obtain an averaged Lagrangian [55]. The variational equations of this averaged Lagrangian then give the modulation equations, ordinary differential equations, describing the evolution of the parameters of the nematicon and vortex, so that their refraction is modelled [51, 58] The only complication in the calculation of these averaged Lagrangians occurs for the

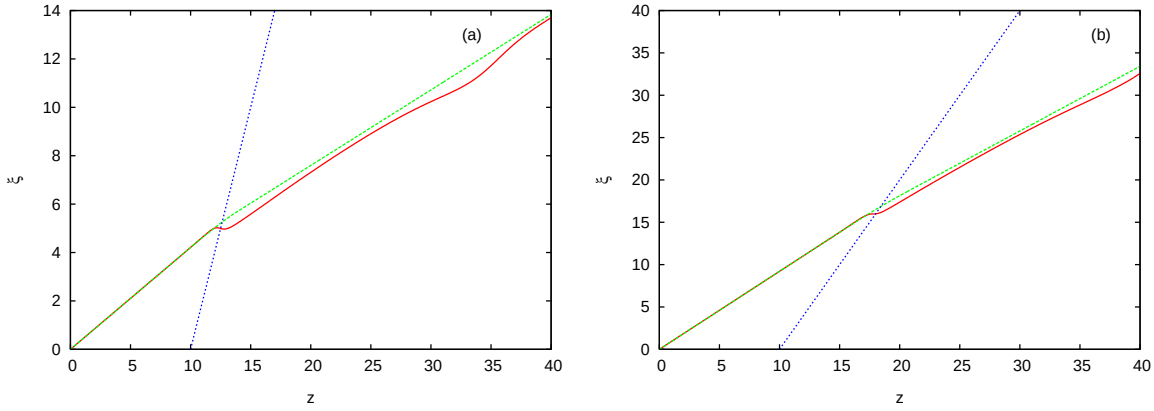

FIG. 6: (Color online) Comparison between nematicon trajectories as given by the full numerical and modulation solutions for the initial values $a = 4.5$ and $w = 2.5$, with $\nu = 200$, $\psi_{bl} = 0.4$, $\psi_{br} = 0.9$, $q_l = 1.0$, $q_r = 1.3$, $\mu_1 = 2$ and $\mu_2 = -20$. Full numerical solution: — (red, solid line); modulation solution: – – – (green, dashed line); interface: - - - - (blue, dotted line). (a) $V_0 = 0.5$, (b) $V_0 = 1.0$.

vortex Lagrangian (10). The Green's function G for the director equation (2) involves modified Bessel functions, which present difficulties when the integrals involved in the averaged Lagrangian are calculated. To overcome this, the nonlocal nature of the director response is employed.

For the large nonlocality ν used in the present work, the response of the director to the optical beam extends far beyond the beam, so that the beam can be approximated as a delta function at the peak $r = w$ of the vortex, relative to the director response [46, 48]. An additional consequence of the nonlocal response of the nematic is that the director distribution is slowly varying, so that within the core of the vortex, $r \leq w$, θ can be taken to be constant as the first term in a Taylor series in $r/\sqrt{\nu}$. This can be seen from the solution of the director equation (2) as the argument of the Bessel function solution is $r\sqrt{2q}/\sqrt{\nu}$. The final approximation needed to obtain an asymptotic solution of the director equation which can be used to exactly calculate the integrals involved in the averaged Lagrangian is that the vortices used in the present work are wide enough to be stable [46]. In this case, the derivative θ_r/r in the director equation (2) can be neglected. With these approximations, the solution of the director equation (2) is

$$\theta = \begin{cases} \frac{a^2 w^3 \sin(2\psi_b)}{4\sqrt{2q\nu}}, & r < w, \\ \frac{a^2 w^3 \sin(2\psi_b)}{4\sqrt{2q\nu}} e^{-\beta(r-w)}, & r \geq w \end{cases} \tag{11}$$

for ν large, where $\beta = \sqrt{2q/\nu}$. In calculating the averaged Lagrangian from (10) ψ_b and q are chosen as either ψ_{bl}, q_l or ψ_{br}, q_r, depending on whether $y > \mu_1 z + \mu_2$ or $y < \mu_1 z + \mu_2$. Due to the discontinuities in ψ_b and q across $y = \mu_1 z + \mu_2$ the integrals with θ involved in calculating the vortex averaged Lagrangian from (10) cannot be evaluated exactly unless $\psi_{bl} = \psi_{br}$ and $q_l = q_r$, in which case there would be no refraction. The director solution (11) for $r > w$ is then extended into $r \leq w$, in which case all these integrals can be evaluated [58]. This introduces an error $O(\nu^{-1/2})$, which is small in the nonlocal limit.

With these approximations, the averaged Lagrangians, and hence the modulation equations governing the refraction of a nematicon and an optical vortex, can be calculated [51, 58]. The actual modulation equations are detailed in the Appendices.

III. RESULTS

Full numerical solutions of the nematicon equations (1) and (2) will now be compared with solutions of the modulation equations of Appendices A and B. The electric field equation (1) was solved using the pseudo-spectral method of Fornberg and Whitham [59], while the director equation (2) was solved using a Fourier method [60]. However, the director angle ψ_b and the pre-tilting electric field q have jump discontinuities across $y = \mu_1 z + \mu_2$. To avoid spurious numerical effects due to these discontinuities both ψ_b and q were smoothed across $y = \mu_1 z + \mu_2$ using a hyperbolic tangent profile linking the levels ψ_{bl}, ψ_{br} and q_l, q_r. The modulation equations of Appendices A and B were solved using the standard fourth order Runge-Kutta scheme [60]. The position of the maximum of the nematicon was used for its numerical position ξ. As the vortex undergoes significant distortions upon refraction, its numerical position

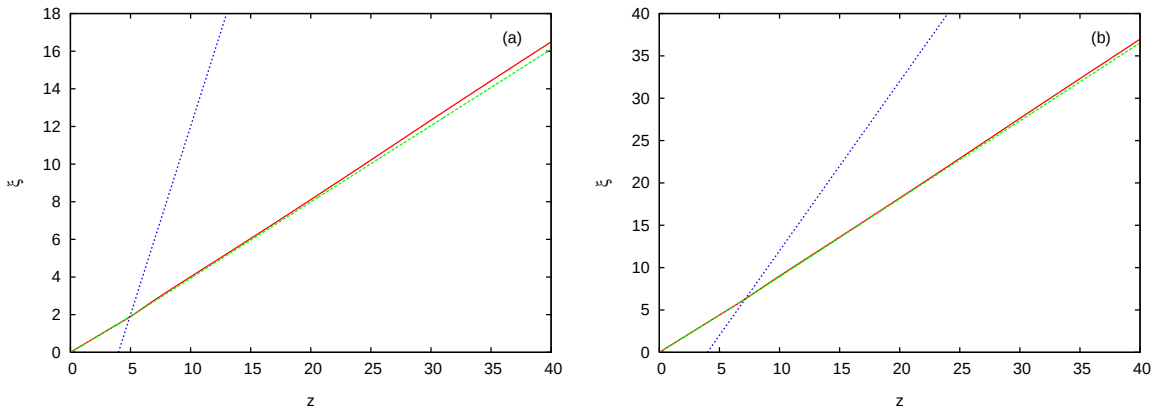

FIG. 7: (Color online) Comparison between nematicon trajectories as given by the full numerical and modulation solutions for the initial values $a = 5.0$ and $w = 2.0$, with $\nu = 200$, $\psi_{bl} = 0.8$, $\psi_{br} = 0.6$, $q_l = 1.3$, $q_r = 1.0$, $\mu_1 = 2$ and $\mu_2 = -8$. Full numerical solution: — (red, solid line); modulation solution: – – – (green, dashed line); interface: - - - - (blue, dotted line). (a) $V_0 = 0.5$, (b) $V_0 = 1.0$.

was estimated using its centre of mass

$$\xi = \frac{\int_{-\infty}^{\infty}\int_{-\infty}^{\infty} y|E|^2\,dxdy}{\int_{-\infty}^{\infty}\int_{-\infty}^{\infty} |E|^2\,dxdy}. \tag{12}$$

Let us compare and contrast the refraction of nematicons and optical vortices. Figures 4 and 5 show the refracted propagation constants $V_f - \Delta_r$ as functions of the incident propagation constants $V_0 - \Delta_l$ for a nematicon and a vortex, respectively. The propagation constants are related to the tangent of the angles of incidence and refraction. These comparisons are shown for refraction both to a less and to a more optically dense medium. It can be seen that for both types of refraction the agreement between the numerical and modulation solutions is similar, with excellent agreement seen. In the case of refraction to a less optically dense medium there are, however, increasing differences between the numerical and modulation solutions as the incident propagation constant increases. As the propagation constant of the nematicon increases, the nematicon evolution changes from refraction to total internal reflection, as for the geometric (ray) optics refraction of light to a less dense medium. However, a nematicon is an extended body and so can overlap the different media on both sides of the interface when it is in its vicinity. This has two consequences, giving two different types of total internal reflection [24, 25]. One is reflection with enhanced Goos-Hänchen shift [32], whereby the nematicon peak enters the less dense medium, but then re-enters the original medium, resulting in total internal reflection. The second is when the beam undergoes total internal reflection without its peak touching the interface, due to its tail crossing the interface and entering the less dense medium. Previous work has found that the intervals of $V_0 - \Delta_l$ for which these different types of refraction and total internal reflection occur are well predicted by modulation theory [51].

The modulation theory outlined in the previous section assumes that the nematicon or vortex is a point particle which does not change its profile, or functional form, as it evolves. While this is an excellent approximation in a uniform medium [36], in a non-uniform case the changes in medium properties can lead to significant beam deformation not accounted for in the modulation theory [44, 45]. Such beam deformations can have an effect on the refraction of nematicons and vortices, relatively minor for the former, but potentially drastic for the latter [58]. Let us now compare and contrast the effect of deformations on the refraction of nematicons and optical vortices.

Figure 6 shows typical nematicon trajectories for low and high angles of incidence for refraction to a denser medium, while Figure 7 shows the equivalent trajectories for refraction to a less dense medium. As the comparisons in Figure 4 show, there is excellent overall agreement between the trajectories as given by the full numerical and modulation solutions. However, it can be seen from Figure 6 that on refraction to the optically denser medium, the numerical nematicon trajectory shows a sudden change. This is explored further in Figure 8 which shows contour plots at $x = 0$ of the evolution of the nematicon on refraction to more and to less dense media. It can be seen from Figure 8(a) that on refraction to the denser region the nematicon has undergone significant distortion, then taking a significant distance to settle back to a uniform state, after which the numerical trajectory returns to the modulation one, as visible in Figure 6(a). The distortion of the nematicon occurs when it is close to the interface, so that different portions of it are in both media. This introduces gradients across its profile, resulting in the distortion, an effect which has been noted in studying the refraction of nematicons by localised refractive index changes [44].

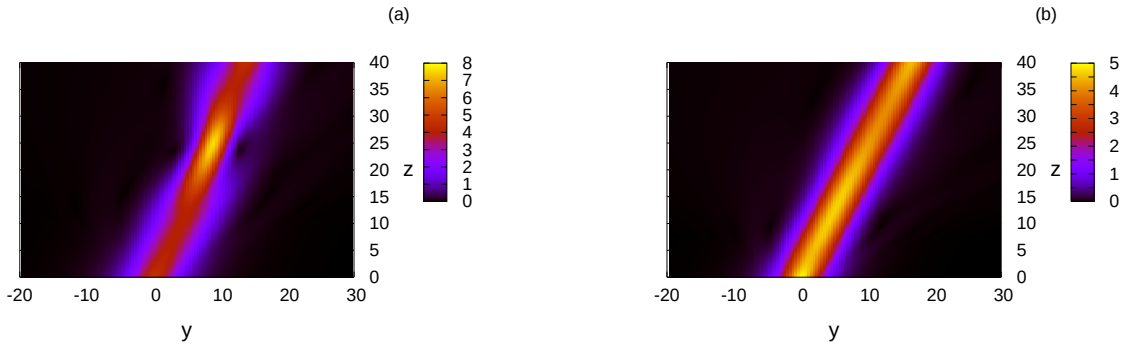

FIG. 8: (Color online) Nematicon evolution at $x = 0$ as given by the full numerical solution for the initial value $V_0 = 0.5$, with $\nu = 200$. (a) Initial values $a = 4.5$, $w = 2.5$, with $\psi_{bl} = 0.4$, $\psi_{br} = 0.9$, $q_l = 1.0$, $q_r = 1.3$, $\mu_1 = 2$ and $\mu_2 = -20$, (b) Initial values $a = 5.0$, $w = 2.0$, with $\psi_{bl} = 0.8$, $\psi_{br} = 0.6$, $q_l = 1.3$, $q_r = 1.0$, $\mu_1 = 2$ and $\mu_2 = -8$

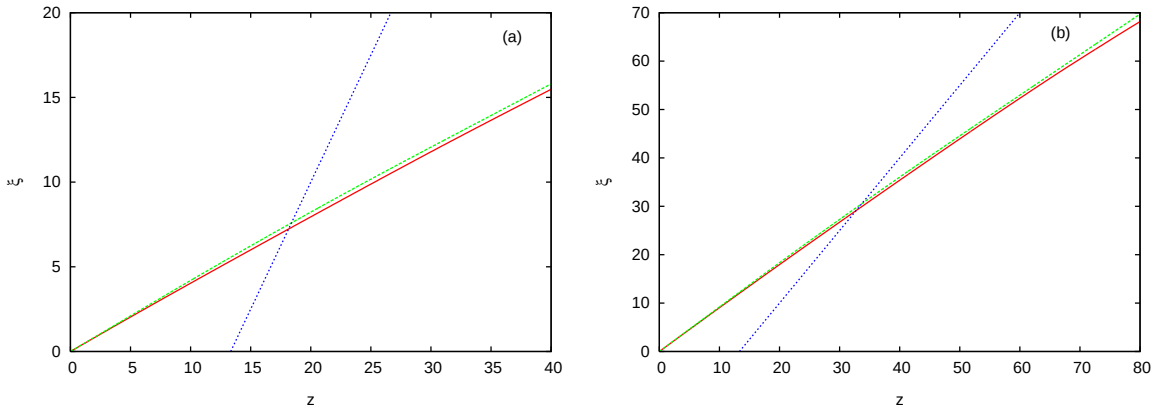

FIG. 9: (Color online) Comparison between vortex trajectories as given by the full numerical and modulation solutions for the initial values $a = 0.15$ and $w = 8.0$, with $\nu = 200$, $\psi_{bl} = 0.4$, $\psi_{br} = 0.9$, $q_l = 1.0$, $q_r = 1.3$, $\mu_1 = 1.5$ and $\mu_2 = -20$. Full numerical solution: — (red, solid line); modulation solution: – – – (green, dashed line); interface: - - - - (blue, dotted line). (a) $V_0 = 0.5$, (b) $V_0 = 1.0$.

It can be appreciated from Figures 7 and 8(b) that there is little distortion of the nematicon on refraction to the less optically dense medium and that there is no corresponding abrupt change in its numerical trajectory. The reason for this is that there is a smaller change in medium properties for the parameter values used, with the change in ψ_b significantly less. This smaller change in properties means that there is a smaller gradient across the beam when it is near the interface, resulting in reduced distortion. The modulation theory approximation of a fixed beam profile is then good, which explains the excellent agreement visible in Figure 4(b) for nematicon refraction over all types from standard refraction, Goos-Hänchen shifted reflection and total internal reflection.

Let us now consider the equivalent refraction of an optical vortex at the interface $y = \mu_1 z + \mu_2$. Figure 5 shows the propagation constant after refraction $V_f - \Delta_r$ as a function of the input propagation constant $V_0 - \Delta_l$. There is again excellent agreement over the entire range between the numerical and modulation results for refraction to an optically denser region and excellent agreement for refraction to a less dense medium up to around $V_0 - \Delta_l = 0.9$. The reasons for this increasing difference between the numerical and modulation results is more complicated than the simple distortion for the refraction of a nematicon and will be discussed in detail below. Figures 9 and 10 display typical trajectory comparisons for vortex refraction to both more and less optically dense media. There are excellent comparisons between the numerical and modulation trajectories in all cases, with the agreement similar to that for the refraction of a nematicon. It should be noted that in Figure 10(b) the vortex is close to total internal reflection. While from the previous discussion it would appear that the vortex is undergoing less distortion than a nematicon, this is not the case, however, due to fundamental differences between the stability of a nematicon and an optical vortex.

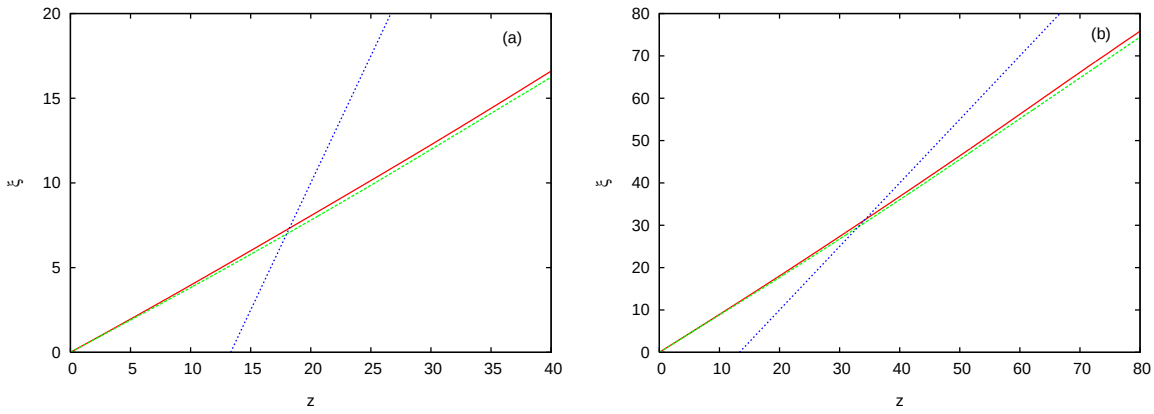

FIG. 10: (Color online) Comparison between vortex trajectories as given by the full numerical and modulation solutions for the initial values $a = 0.15$ and $w = 8.0$, with $\nu = 200$, $\psi_{bl} = 0.8$, $\psi_{br} = 0.4$, $q_l = 1.3$, $q_r = 1.0$, $\mu_1 = 1.5$ and $\mu_2 = -20$. Full numerical solution: — (red, solid line); modulation solution: – – – (green, dashed line); interface: - - - - (blue, dotted line). (a) $V_0 = 0.5$, (b) $V_0 = 1.0$.

Unlike a nematicon, an optical vortex has an azimuthal structure, as seen in the trial function (8). If the nonlocality ν is not large enough, the charge 1 vortex can then have a mode two azimuthal instability which results in its breaking up into two nematicons [46, 61], as recently reported in experiments [62]. For the parameter values used here, in particular the nonlocality $\nu = 200$, the optical vortices are stable in the uniform media on either side of the interface. However, the interaction with the interface triggers the mode 2 azimuthal instability. Figure 11 shows numerical vortex solutions well after it has crossed the interface for refraction to both more and less optically dense media. The mode 2 azimuthal wave can be clearly seen, with the azimuthal perturbation being larger for refraction to the less dense medium. In addition to the vortices, the diffractive radiation shed by them as they evolve can be clearly seen. By shedding radiation, the vortices can evolve to a steady state of a circumferentially uniform vortex. The longer distance that the vortex spends in the interface vicinity, the stronger the mode 2 instability. Figure 12 shows the same initial vortex as in Figure 11(b), but for $V_0 = 1.3$ rather than $V_0 = 1$. At $z = 120$ the interface is at $y = 160$ and at $z = 200$ the interface is at $y = 280$. Figure 12(a) shows that the vortex initially breaks up into two nematicons, one on either side of the interface, due to the forcing of the mode 2 instability. Then remnants of the vortex linking these two nematicons form into a third nematicon on the incident side of the interface, as seen in Figure 12(b). For $V = 1.3$ the vortex is close to total internal reflection and its trajectory is in close proximity to the interface for an extended distance. The instability is then forced sufficiently to fully trigger it, leading to the vortex breakup, in contrast to the cases of Figure 11 for which the vortices are not close to the interface for a long enough distance to become unstable. Numerical solutions show that the vortex becomes unstable at $V_0 = 1.1$, in good agreement with the modulation prediction of $V_0 = 1.18$. The refraction of an optical vortex to a less optically dense medium then does not show Goos-Hänchen shift upon reflection and standard total internal reflection as the instability is triggered before these can occur. The instability of the vortex for $V_0 > 1.1$, or $V_0 - \Delta_l > 0.9803$, explains the increasing difference visible in the comparison of Figure 5(b) for $V_0 - \Delta_l > 0.9$.

IV. CONCLUSIONS

Modulation theory is an elegant theoretical tool for the modelling of complex phenomena in linear and nonlinear optics. Its application to anisotropic and nonlocal dielectrics with a reorientational nonlinear response, namely nematic liquid crystals, leads to excellent qualitative agreement with experimental results and excellent quantitative agreement with numerical results for the evolution of self-confined light beams even in the presence of an interface separating two optically unequal regions in terms of the orientation of the optic axis. The modulation theory results on the refraction and total internal reflection of nematicons are consistent with experimental data and numerical simulations, even when accounting for birefringent walkoff. Moreover, our modulation theory study of optical vortices in nematic liquid crystals leads to the prediction that their azimuthal instability and their break-up into bright beams can be triggered by reflection off an interface, an effect awaiting experimental validation.

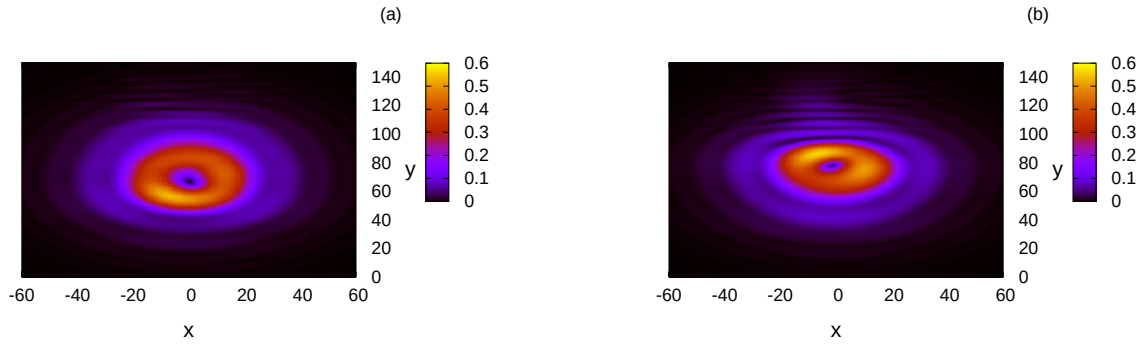

FIG. 11: (Color online) Numerical solution $|E|$ for vortex at $z = 120$ for initial values $a = 0.15$, $w = 8.0$ and $V_0 = 1.0$, with $\nu = 200$. (a) $\psi_{bl} = 0.4$, $\psi_{br} = 0.9$, $q_l = 1.0$, $q_r = 1.3$, $\mu_1 = 2$ and $\mu_2 = -80$, (b) $\psi_{bl} = 0.8$, $\psi_{br} = 0.4$, $q_l = 1.3$, $q_r = 1.0$, $\mu_1 = 1.5$ and $\mu_2 = -20$.

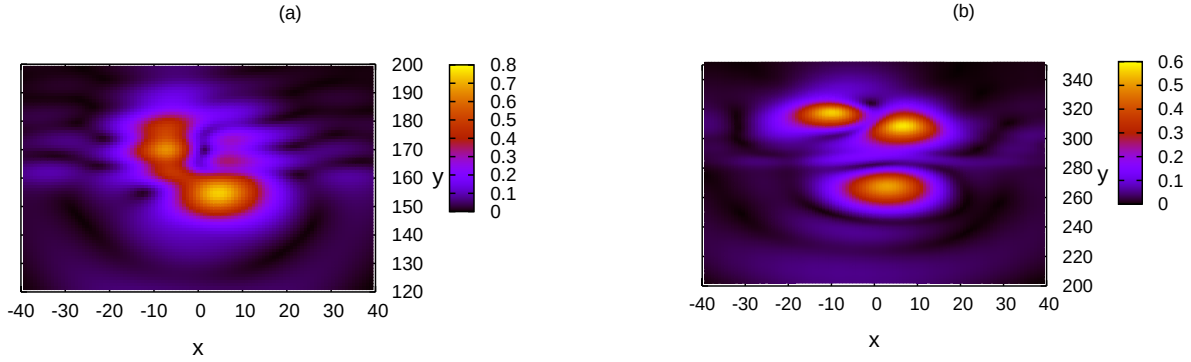

FIG. 12: (Color online) Numerical solution $|E|$ for vortex for initial values $a = 0.15$, $w = 8.0$ and $V_0 = 1.3$, with $\nu = 200$, $\psi_{bl} = 0.8$, $\psi_{br} = 0.4$, $q_l = 1.3$, $q_r = 1.0$, $\mu_1 = 1.5$ and $\mu_2 = -20$. (a) $z = 120$, (b) $z = 200$.

Appendix A: Modulation Equations for Nematicons

$$\frac{d}{dz}\left(I_2 a^2 w^2 + \Lambda g^2\right) = 0, \tag{A1}$$

$$\frac{d\xi}{dz} = V - \frac{1}{2}\left[\Delta_l \operatorname{erfc}(\lambda_2) + \Delta_r \operatorname{erfc}(-\lambda_2)\right], \tag{A2}$$

$$\frac{dV}{dz} = \frac{BV}{2\sqrt{\pi} I_2 w}\left(\Delta_l - \Delta_r\right) e^{-\lambda_2^2} + \frac{AB\alpha\beta}{2\sqrt{\pi} I_2 w\sqrt{Q}}\left(\sin 2\psi_{bl} - \sin 2\psi_{br}\right) e^{-\lambda_1^2} - \frac{\sqrt{2} D\alpha^2\beta}{4\sqrt{\pi} I_2 a^2 w^2}\left(q_l - q_r\right) e^{-\lambda_3^2}, \tag{A3}$$

$$I_1 \frac{d}{dz} a w^2 = \Lambda g\left(\sigma' - V\xi' + \frac{1}{2}V^2\right), \tag{A4}$$

$$I_1 \frac{dg}{dz} = \frac{I_{22} a}{2w^2} - \frac{A^2 B^4 \alpha\beta^2 a w^2}{4Q^2}\left[\sin(2\psi_{bl}) \operatorname{erfc}(\lambda_1) + \sin(2\psi_{br}) \operatorname{erfc}(-\lambda_1)\right]$$
$$+ \frac{A^3 B\alpha\beta^3 a}{4\sqrt{\pi} w Q^{3/2}}\left[\sin 2\psi_{bl} - \sin 2\psi_{br}\right] e^{-\lambda_1^2} + \frac{BaV}{4\sqrt{\pi} w}\left(\mu_1 z + \mu_2 - \xi\right)\left(\Delta_l - \Delta_r\right) e^{-\lambda_2^2}, \tag{A5}$$

$$\frac{d\sigma}{dz} - V\frac{d\xi}{dz} + \frac{1}{2}V^2 = -\frac{I_{22}}{I_2 w^2}$$
$$+ \frac{A^2\alpha\beta^2\left(A^2\beta^2 + 2B^2w^2\right)}{2Q^2}\left[\sin(2\psi_{bl})\,\mathrm{erfc}(\lambda_1) + \sin(2\psi_{br})\,\mathrm{erfc}(-\lambda_1)\right]$$
$$- \frac{A^3B\alpha\beta^3}{4I_2wQ^{3/2}}\left(\sin 2\psi_{bl} - \sin 2\psi_{br}\right)e^{-\lambda_1^2} + \frac{1}{2}V\left[\Delta_l\,\mathrm{erfc}(\lambda_2) + \Delta_r\,\mathrm{erfc}(-\lambda_2)\right]$$
$$- \frac{BV}{4\sqrt{\pi}I_2 w}\left(\mu_1 z + \mu_2 - \xi\right)\left(\Delta_l - \Delta_r\right)e^{-\lambda_2^2}, \tag{A6}$$

together with the algebraic equations

$$\alpha = \frac{A^2B^2\beta^2a^2w^2}{Q}\frac{\sin(2\psi_{bl})\,\mathrm{erfc}(\lambda_1) + \sin(2\psi_{br})\,\mathrm{erfc}(-\lambda_1)}{16\nu I_{42} + D^2\beta^2\left[q_l\,\mathrm{erfc}(\lambda_3) + q_r\,\mathrm{erfc}(-\lambda_3)\right]}, \tag{A7}$$

$$\frac{A^2B^4\beta a^2w^4}{Q^2}\left[\sin(2\psi_{bl})\,\mathrm{erfc}(\lambda_1) + \sin(2\psi_{br})\,\mathrm{erfc}(-\lambda_1)\right]$$
$$+ \frac{AB^3a^2w^3}{\sqrt{\pi}Q^{3/2}}\left(\sin 2\psi_{bl} - \sin 2\psi_{br}\right)\left(\mu_1 z + \mu_2 - \xi\right)e^{-\lambda_1^2}$$
$$- \frac{1}{2}D^2\alpha\beta\left[q_l\,\mathrm{erfc}(\lambda_3) + q_r\,\mathrm{erfc}(-\lambda_3)\right] - \frac{D}{\sqrt{2\pi}}\alpha(q_l - q_r)\left(\mu_1 z + \mu_2 - \xi\right)e^{-\lambda_3^2} = 0. \tag{A8}$$

Here

$$\Lambda = \frac{1}{2}R^2, \quad Q = A^2\beta^2 + B^2w^2, \tag{A9}$$
$$\lambda_1 = \frac{\sqrt{A^2\beta^2 + B^2w^2}}{AB\beta w}\left(\mu_1 z + \mu_2 - \xi\right), \quad \lambda_2 = \frac{\mu_1 z + \mu_2 - \xi}{Bw}, \quad \lambda_3 = \frac{\sqrt{2}\left(\mu_1 z + \mu_2 - \xi\right)}{D\beta}$$

and

$$I_1 = 2C, \quad I_2 = \ln 2, \quad I_{22} = \frac{1}{3}\ln 2 + \frac{1}{6}, \quad I_{x32} = 1.352314016\ldots, \quad I_{42} = \frac{2}{15}\ln 2 + \frac{1}{60}, \quad I_4 = \frac{2}{3}\ln 2 - \frac{1}{6},$$
$$A = \frac{I_2\sqrt{2}}{\sqrt{I_{x32}}}, \quad B = \sqrt{2I_2} \quad \text{and} \quad D = 2\sqrt{I_4}. \tag{A10}$$

Here C is the Catalan constant $C = 0.915965594\ldots$ [63].

Appendix B: Modulation Equations for Vortices

$$\frac{d}{dz}\left[\frac{3}{8}a^2w^4 + \Lambda_1 g^2\right] = 0, \tag{B1}$$
$$4\frac{d}{dz}\left(aw^3\right) = 2\Lambda_1 g\left[\sigma' - V\xi' + \frac{1}{2}V^2\right] + \Lambda_2 g, \tag{B2}$$
$$\frac{d\xi}{dz} = V - \frac{1}{2}\left[\Delta_l\,\mathrm{erfc}(\lambda_1) + \Delta_r\,\mathrm{erfc}(-\lambda_1) + \frac{\lambda_1}{\sqrt{\pi}}\left(\Delta_l - \Delta_r\right)e^{-\lambda_1^2}\right], \tag{B3}$$
$$4\frac{d}{dz}\left[\frac{3}{8}a^2w^4 + \Lambda_1 g^2\right]V = \frac{A_1^3}{\sqrt{\pi}}a^2w^3V\left(\Delta_l - \Delta_r\right)\left(1 + 2\lambda_1^2\right)e^{-\lambda_1^2}$$
$$- \sin^2(2\psi_{bl})\frac{a^4w^3e^{\beta_l w - \lambda_l^2}}{4A_2^3\sqrt{2\pi q_l\nu}}\left(\beta_l + \frac{2}{w}\right)^{-3}\left(\frac{1}{2} + \lambda_l^2\right)$$
$$+ \sin^2(2\psi_{br})\frac{a^4w^3e^{\beta_r w - \lambda_r^2}}{4A_2^3\sqrt{2\pi q_r\nu}}\left(\beta_r + \frac{2}{w}\right)^{-3}\left(\frac{1}{2} + \lambda_r^2\right), \tag{B4}$$

$$\frac{dg}{dz} = \frac{3}{32}\frac{a}{w} + \frac{3\lambda_1 V a w}{64\sqrt{\pi}}\left(\Delta_l - \Delta_r\right)\left(1+2\lambda_1^2\right)e^{-\lambda_1^2} \tag{B5}$$
$$+\sin^2(2\psi_{bl})\frac{3a^3 e^{\beta_l w}}{32w\sqrt{2q_l\nu}}\left(\beta_l+\frac{2}{w}\right)^{-5}\left[\frac{1}{\sqrt{\pi}}\left(\beta_l^2w^2-3\beta_l w+4\lambda_l^2\right)\lambda_l e^{-\lambda_l^2}-\left(2+3\beta_l w-\beta_l^2w^2\right)\mathrm{erfc}(\lambda_l)\right]$$
$$-\sin^2(2\psi_{br})\frac{3a^3 e^{\beta_r w}}{32w\sqrt{2q_r\nu}}\left(\beta_r+\frac{2}{w}\right)^{-5}\left[\frac{1}{\sqrt{\pi}}\left(\beta_r^2w^2-3\beta_r w+4\lambda_r^2\right)\lambda_r e^{-\lambda_r^2}+\left(2+3\beta_r w-\beta_r^2w^2\right)\mathrm{erfc}(-\lambda_r)\right],$$

$$\frac{d\sigma}{dz} - V\frac{d\xi}{dz} + \frac{1}{2}V^2 = -w^{-2} + \frac{1}{4}V\left[2\Delta_l\,\mathrm{erfc}(\lambda_1) + 2\Delta_r\,\mathrm{erfc}(-\lambda_1) + \frac{1}{\sqrt{\pi}}\left(\Delta_l-\Delta_r\right)\left(1-2\lambda_1^2\right)\lambda_1 e^{-\lambda_1^2}\right]$$
$$+\sin^2(2\psi_{bl})\frac{a^2 e^{\beta_l w}}{2w^2\sqrt{2q_l\nu}}\left(\beta_l+\frac{2}{w}\right)^{-5}\left[\frac{1}{\sqrt{\pi}}\left(8+7\beta_l w-\beta_l^2w^2-4\lambda_l^2\right)\lambda_l e^{-\lambda_l^2}+\left(10+7\beta_l w-\beta_l^2w^2\right)\mathrm{erfc}(\lambda_l)\right]$$
$$-\sin^2(2\psi_{br})\frac{a^2 e^{\beta_r w}}{2w^2\sqrt{2q_r\nu}}\left(\beta_r+\frac{2}{w}\right)^{-5}\times$$
$$\left[\frac{1}{\sqrt{\pi}}\left(8+7\beta_r w-\beta_r^2w^2-4\lambda_r^2\right)\lambda_r e^{-\lambda_r^2}-\left(10+7\beta_r w-\beta_r^2w^2\right)\mathrm{erfc}(-\lambda_r)\right]$$

Here

$$\Lambda_1 = w^2, \quad \Lambda_2 = \ln 3, \quad \beta_l = \sqrt{\frac{2q_l}{\nu}}, \quad \beta_r = \sqrt{\frac{2q_r}{\nu}},$$
$$\lambda_1 = \frac{\mu_1 z+\mu_2-\xi}{A_1 w}, \quad \lambda_l = A_2\left(\beta_l+\frac{2}{w}\right)\left(\mu_1 z+\mu_2-\xi\right), \quad \lambda_r = A_2\left(\beta_r+\frac{2}{w}\right)\left(\mu_1 z+\mu_2-\xi\right),$$
$$A_1 = \left(\frac{3}{4}\right)^{1/4}, \quad A_2 = 12^{-1/4}. \tag{B6}$$

[1] G. Assanto, A. Fratalocchi and M. Peccianti, "Spatial solitons in nematic liquid crystals: from bulk to discrete," *Opt. Express,* **15**, 5248–5259 (2007).

[2] G. Assanto and M. Karpierz, "Nematicons: self-localized beams in nematic liquid crystals," *Liq. Cryst.,* **36**, 1161–1172 (2009).

[3] M. Peccianti and G. Assanto, "Nematicons," *Phys. Rep.,* doi:10.1016/j.physrep.2012.02.004 (2012).

[4] M. Peccianti, G. Assanto, A. De Luca, C. Umeton, and I.C. Khoo, "Electrically assisted self-confinement and waveguiding in planar nematic liquid crystal cells," *Appl. Phys. Lett.,* **77**, 7–9 (2000).

[5] M. Peccianti and G. Assanto, "Signal readdressing by steering of spatial solitons in bulk Nematic Liquid Crystals," *Opt. Lett.,* **26**, 1690–1692 (2001).

[6] Y. V. Izdebskaya, A. S. Desyatnikov, G. Assanto, and Y. S. Kivshar, "Multimode nematicon waveguides," *Opt. Lett.,* **36**, 184–186 (2011).

[7] M. Peccianti, A. Fratalocchi and G. Assanto, "Transverse dynamics of nematicons," *Opt. Express,* **12**, 6524–6529 (2004).

[8] M. Peccianti, C. Conti, G. Assanto, A. De Luca and C. Umeton, "Routing of Highly Anisotropic Spatial Solitons and Modulational Instability in liquid crystals," *Nature,* **432**, 733–737 (2004).

[9] G. Assanto, C. Umeton, M. Peccianti and A. Alberucci, "Nematicons and their angular steering," *J. Nonl. Opt. Phys. Mat.,* **15**, 33–42 (2006).

[10] A. Piccardi, M. Peccianti, G. Assanto, A. Dyadyusha and M. Kaczmarek, "Voltage-driven in-plane steering of nematicons," *Appl. Phys. Lett.,* **94**, 091106 (2009)

[11] A. Piccardi, U. Bortolozzo, S. Residori and G. Assanto, "Spatial solitons in liquid crystal light valves," *Opt. Lett.,* **34**, 737-739 (2009).

[12] A. Piccardi, A. Alberucci and G. Assanto, "Soliton self-deflection via power-dependent walk-off," *Appl. Phys. Lett.,* **96**, 061105 (2010).

[13] M. Peccianti, K. A. Brzdakiewicz, and G. Assanto, "Nonlocal spatial soliton interactions in bulk nematic liquid crystals," *Opt. Lett.,* **27**, 1460–1462 (2002).

[14] M. Peccianti, C. Conti, G. Assanto, A. De Luca and C. Umeton, "All Optical Switching and Logic Gating with Spatial Solitons in Liquid Crystals," *Appl. Phys. Lett.,* **81**, 3335–3337 (2002).

[15] Y. V. Izdebskaya, V. G. Shvedov, A. S. Desyatnikov, W. Z. Krolikowski, M. Belic, G. Assanto, and Y. S. Kivshar, "Counterpropagating nematicons in bias-free liquid crystals," *Opt. Express,* **18**, 3258–3263 (2010).

[16] A. Alberucci, M. Peccianti, G. Assanto, A. Dyadyusha and M. Kaczmarek, "Two-color vector solitons in non local media," *Phys. Rev. Lett.,* **97**, 153903 (2006).

[17] A. Pasquazi, A. Alberucci, M. Peccianti and G. Assanto, "Signal processing by opto-optical interactions between self-localized and free propagating beams in liquid crystals," *Appl. Phys. Lett.,* **87**, 261104 (2005).

[18] S. V. Serak, N. V. Tabiryan, M. Peccianti and G. Assanto, "Spatial Soliton All-Optical Logic Gates," *IEEE Photon. Techn. Lett.,* **18**, 1287–1289 (2006).

[19] A. Piccardi, A. Alberucci, U. Bortolozzo, S. Residori and G. Assanto, "Readdressable interconnects with spatial soliton waveguides in liquid crystal light valves," *Photon. Techn. Lett.,* **22**, 694–696 (2010).

[20] A. Alberucci and G. Assanto, "Propagation of optical spatial solitons in finite size media: interplay between non locality and boundary conditions," *J. Opt. Soc. Am. B,* **24**, 2314–2320 (2007).

[21] A. Alberucci, M. Peccianti and G. Assanto, "Nonlinear bouncing of nonlocal spatial solitons at the boundaries," *Opt. Lett.,* **32**, 2795–2797 (2007).

[22] M. Peccianti, A. Dyadyusha, M. Kaczmarek, and G. Assanto, "Escaping Solitons from a trapping potential," *Phys. Rev. Lett.,* **101**, 153902 (2008).

[23] Y. V. Izdebskaya, V. Shvedov, A. S.Desyatnikov, W. Krolikowski, and Y.S. Kivshar, "Soliton bending and routing induced by interaction with curved surfaces in nematic liquid crystals," *Opt. Lett.,* **35** 1692–1694 (2010).

[24] M. Peccianti, A. Dyadyusha, M. Kaczmarek and G. Assanto, "Tunable refraction and reflection of self-confined light beams," *Nature Phys.,* **2**, 737–742 (2006).

[25] M. Peccianti, G. Assanto, A. Dyadyusha and M. Kaczmarek, "Nonlinear shift of spatial solitons at a graded dielectric interface," *Opt. Lett.,* **32**, 271–273 (2007).

[26] M. Peccianti and G. Assanto, "Nematicons across interfaces: anomalous refraction and reflection of solitons in liquid crystals," *Opt. Express,* **15**, 8021-8-802 (2007).

[27] M. Peccianti, G. Assanto, A. Dyadyusha and M. Kaczmarek, "Nonspecular total internal reflection of spatial soliton at the interface between highly birefringent media," *Phys. Rev. Lett.,* **98**, 113902 (2007).

[28] A. Piccardi, G. Assanto, L. Lucchetti and F. Simoni, "All-optical steering of soliton waveguides in dye-doped liquid crystals," *Appl. Phys. Lett.,* **93**, 171104 (2008).

[29] R. Barboza, A. Alberucci and G. Assanto, "Large electro-optic beam steering with Nematicons," *Opt. Lett.,* **36**, 2611–2613 (2011).

[30] A. Piccardi, A. Alberucci, R. Barboza, O. Buchnev, M. Kaczmarek and G. Assanto, "In-plane steering of nematicon waveguides across an electrically adjusted interfac," *Appl. Phys. Lett.,* **100**, 251107 (2012).

[31] M. Peccianti, C. Conti and G. Assanto, "The interplay between non locality and nonlinearity in nematic liquid crystals," *Opt. Lett.,* **30**, 415–417 (2005).

[32] F. Goos and H. Hänchen, "Ein neuer und fundamentaler Versuch zur Total reflexion," *Ann. Phys.,* **436**, 333–346 (1947).

[33] G. Assanto, A.A. Minzoni, M. Peccianti and N.F. Smyth, "Optical solitary waves escaping a wide trapping potential in nematic liquid crystals: modulation theory," *Phys. Rev. A,* **79**, 033837 (2009).

[34] C. García-Reimbert, A.A. Minzoni and N.F. Smyth, "Spatial soliton evolution in nematic liquid crystals in the nonlinear local regime," *J. Opt. Soc. Amer. B,* **23**, 294–301 (2006).

[35] C. García-Reimbert, A.A. Minzoni, N.F. Smyth, A.L. Worthy, "Large-amplitude nematicon propagation in a liquid crystal with local response," *J. Opt. Soc. Amer. B,* **23**, 2551–2558 (2006).

[36] A.A. Minzoni, N.F. Smyth and A.L. Worthy, "Modulation solutions for nematicon propagation in non-local liquid crystals," *J. Opt. Soc. Amer. B,* **24**, 1549–1556 (2007).

[37] A.A. Minzoni, L.W. Sciberras, N.F. Smyth and A.L. Worthy, "Propagation of optical spatial solitary waves in bias-free nematic liquid crystal cells," *Phys. Rev. A,* **84**, 043823 (2011).

[38] B.D. Skuse and N.F. Smyth, "Two-colour vector soliton interactions in nematic liquid crystals in the local response regime," *Phys. Rev. A,* **77**, 013817 (2008).

[39] B.D. Skuse and N.F. Smyth, "Interaction of two colour solitary waves in a liquid crystal in the nonlocal regime," *Phys. Rev. A,* **79**, 063806 (2009).

[40] G. Assanto, N.F. Smyth and A.L. Worthy, "Two colour, nonlocal vector solitary waves with angular momentum in nematic liquid crystals," *Phys. Rev. A,* **78**, 013832 (2008).

[41] G. Assanto, C. García-Reimbert, A.A. Minzoni, N.F. Smyth, and A.L. Worthy, "Lagrange solution for three wavelength solitary wave clusters in nematic liquid crystals," *Physica D,* **240**, 1213–1219 (2011).

[42] G. Assanto, B.D. Skuse, and N.F. Smyth, "Optical path control of spatial optical solitary waves in dye-doped nematic liquid crystals," *Photon. Lett. Poland,* **1**, 154–156 (2009).

[43] G. Assanto, B.D. Skuse and N.F. Smyth, "Solitary wave propagation and steering through light-induced refractive potentials," *Phys. Rev. A,* **81**, 063811 (2010).

[44] G. Assanto, A.A. Minzoni, N.F. Smyth and A.L. Worthy, "Refraction of nonlinear beams by localised refractive index changes in nematic liquid crystals," *Phys. Rev. A,* **82**, 053843 (2010).

[45] A. Alberucci, G. Assanto, A.A. Minzoni and N.F. Smyth, 'Scattering of reorientational optical solitary waves at dielectric perturbations," *Phys. Rev. A,* **85**, 013804 (2012).

[46] A.A. Minzoni, N.F. Smyth, A.L. Worthy and Y.S. Kivshar, "Stabilization of vortex solitons in nonlocal nonlinear media," *Phys. Rev. A,* **76**, 063803 (2007).

[47] Z. Xu, N.F. Smyth, A.A. Minzoni and Y.S. Kivshar, "Vector vortex solitons in nematic liquid crystals," *Opt. Lett.,* **34**, 1414–1416 (2009).

[48] A.A. Minzoni, N.F. Smyth, Z. Xu and Y.S. Kivshar, "Stabilization of vortex-soliton beams in nematic liquid crystals,"

Phys. Rev. A, **79**, 063808 (2009).
[49] C. Conti, M. Peccianti and G. Assanto, "Route to nonlocality and observation of accessible solitons," *Phys. Rev. Lett.,* **91**, 073901 (2003).
[50] C. Conti, M. Peccianti and G. Assanto, "Observation of optical spatial solitons in a highly nonlocal medium," *Phys. Rev. Lett.,* **92**, 113902 (2004).
[51] G. Assanto, N.F. Smyth and W. Xia, "Modulation analysis of nonlinear beam refraction at an interface in liquid crystals," *Phys. Rev. A,* **84**, 033818 (2011).
[52] G. Assanto, N.F. Smyth and W. Xia, "Modulation analysis of nonlinear beam refraction at an interface in liquid crystals," *Phys. Rev. A,* **84**, 033818 (2011).
[53] *CRC Handbook of Laser Science and Technology: Optical Materials*, Suppl. 2, ed. M.J. Weber, CRC Press, New York (1995).
[54] W.L. Kath and N.F. Smyth, "Soliton evolution and radiation loss for the nonlinear Schrödinger equation," *Phys. Rev. E,* **51**, 1484–1492 (1995).
[55] G.B. Whitham, *Linear and Nonlinear Waves,* J. Wiley and Sons, New York (1974).
[56] J. Yang, "Vector solitons and their internal oscillations in birefringent nonlinear optical fibers" *Stud. Appl. Math.,* **98**, 61–97 (1997).
[57] M.J. Ablowitz, S.D. Dixon, T.P. Horikis and D.J. Frantzeskakis, "Perturbations of dark solitons," *Proc. R. Soc. Lond. A,* **467**, 2597–2621 (2011).
[58] N.F. Smyth and W. Xia, "Refraction and instability of optical vortices at an interface in a liquid crystal, *J. Phys. B: Atomic, Molec. and Opt. Phys.,* **45**, 165403 (2012).
[59] B. Fornberg and G.B. Whitham, "A numerical and theoretical study of certain nonlinear wave phenomena," *Phil. Trans. R. Soc. Lond. A,* **289**, 373–403 (1978).
[60] W.H. Press, S.A. Teukolsky, W.T. Vetterling, and B.P. Flannery, *Numerical Recipes in Fortran. The Art of Scientific Computing,* Cambridge University Press (1992).
[61] A.I. Yakimenko, Yu.A. Zaliznyak and Yu.S. Kivshar, "Stable vortex solitons in nonlocal self-focusing nonlinear media," *Phys. Rev. E* **71**, 065603(R) (2005).
[62] Y.V. Izdebskaya, A.S. Desyatnikov, G. Assanto and Yu.S. Kivshar, "Dipole azimuthons and charge-flipping in nematic liquid crystals," *Opt. Express* **19**, 21457–66 (2011).
[63] M. Abramowitz and I.A. Stegun, *Handbook of Mathematical Functions with Formulas, Graphs and Mathematical Tables,* Dover Publications, Inc., New York (1972).